

Surface magnetoelectric driven spin dynamics in metallic antiferromagnets

R. M. Dubrovin^{a,*}, A. V. Kimel^b and A. K. Zvezdin^{c,d,*}

^a*Ioffe Institute, Russian Academy of Sciences, 194021 St. Petersburg, Russia*

^b*Institute for Molecules and Materials, Radboud University, 6525 AJ Nijmegen, The Netherlands*

^c*New Spintronic Technologies LLC, 121205 Skolkovo, Moscow, Russia*

^d*Prokhorov General Physics Institute, Russian Academy of Sciences, 119991 Moscow, Russia*

ARTICLE INFO

Keywords:

Magnetoelectric effect
Metallic antiferromagnets
Spin dynamics
Spin switching

ABSTRACT

Although magnetoelectric effects in metals are usually neglected, assuming that applied electric fields are screened by free charge carriers, the skin depth, defining the penetration depth of the fields, is non-zero and for THz electric fields typically reaches 400 nm. Hence, if the thickness of an antiferromagnetic film is of the order of tens of nm, electric field induced effects cannot be neglected. Here, we theoretically study the THz electric field induced spin dynamics in the metallic antiferromagnets Mn₂Au and CuMnAs, whose spin arrangements allow them to exhibit a linear magnetoelectric effect. We show that the THz magnetoelectric torque in metallic antiferromagnets is proportional to the time derivative of the THz electric field induced polarization. Our calculations reveal that the magnetoelectric driven spin dynamics is indeed not negligible and can fairly explain the previously published experimental results on antiferromagnetic dynamics excited by the THz pump pulses in Mn₂Au at the corresponding magnetoelectric susceptibility value $\alpha_{ME} \simeq 2 \times 10^{-5}$ without involving other mechanisms. This value is about one order of magnitude smaller than that known for collinear and rare-earth-free antiferromagnets such as Cr₂O₃. For such a value of magnetoelectric response, it appears that the THz electric fields of realistic strengths of about 1 MV/cm are sufficient in order to achieve spin dynamics with the amplitudes sufficiently strong enough for switching of the antiferromagnetic Néel vector between the stable ground states. Thus, we contend that the experimental studies of the coherent dynamics of the antiferromagnetic vector driven by the THz pulses in magnetoelectric metal films necessitate a careful consideration of the linear magnetoelectric effect.

1. Introduction

Antiferromagnets form the largest, least explored, but probably the most intriguing class of magnetic materials promising to revolutionize spintronic technologies. In particular, it is believed that the use of antiferromagnets can push the rates of processing magnetically stored data to the THz domain [1, 2, 3, 4, 5]. In the simplest case, an antiferromagnet is described as two antiferromagnetically coupled and completely equivalent ferromagnetic sublattices, with magnetizations \mathbf{m}_A and \mathbf{m}_B , respectively. The antiferromagnetic order parameter in this case is the antiferromagnetic Néel vector $\mathbf{I} \propto \mathbf{m}_A - \mathbf{m}_B$. Finding the mechanisms allowing to control spins in antiferromagnets has been as a challenge from the discovery of antiferromagnetism because neither electric nor magnetic field seems to couple to the order parameter, at least in the simplest model of antiferromagnet, a $\mathbf{I} \cdot \mathbf{H} = 0$ and $\mathbf{I} \cdot \mathbf{E} = 0$.

There are two prototypical antiferromagnetic metallic spintronic materials, Mn₂Au and CuMnAs, in which the breaking of the inversion \mathcal{I} and time-reversal \mathcal{T} symmetry, while their combination \mathcal{IT} is preserved and connects two oppositely aligned Mn magnetic sublattices, leading to a linear magnetoelectric effect [6, 7] and allowing to couple the elec-

tric field \mathbf{E} to the antiferromagnetic order parameter \mathbf{I} as in the case of insulating Cr₂O₃ [8, 9, 10]. In metals and semimetals, the free carriers screen an externally applied electric field at depths greater than the skin depth, and the linear magnetoelectric effect is therefore negligible. On the other hand, materials with the symmetry that allows magnetoelectric effect may also possess magnetogalvanic effects, where the antiferromagnetic Néel vector is coupled to an electrical current [11, 12]. Switching of the antiferromagnetic Néel vector \mathbf{I} between allowed ground states under the influence of charge and spin-polarized currents has been predicted and experimentally demonstrated in the metals Mn₂Au and CuMnAs via the Néel spin-orbit torque [13, 14, 15], as well as quench switching [16, 17] mechanisms. However, in thin films of Mn₂Au and CuMnAs with a thickness less than the skin depth, roughly estimated at about 400 nm for the 1 THz radiation [18], the applied THz electric field penetrates into the material, which should also result in a magnetoelectric response.

Here, we present a theoretical study of the THz driven spin dynamics in the metallic magnetoelectric antiferromagnets Mn₂Au and CuMnAs films with a thickness less than the skin depth. Employing the Lagrangian approach, we derive differential equations that take into account the linear magnetoelectric effect and describe the coherent dynamics of the antiferromagnetic Néel vector \mathbf{I} near the ground state under the action of the electric and magnetic fields of THz pulses. We show that our model, taking into account only the

*Corresponding authors.

 dubrovin@mail.ioffe.ru (R.M. Dubrovin);

zvezdin.ak@phystech.edu (A.K. Zvezdin)

ORCID(s): 0000-0002-7235-7805 (R.M. Dubrovin);

0000-0002-0709-042X (A.V. Kimel); 0000-0002-6039-780X (A.K. Zvezdin)

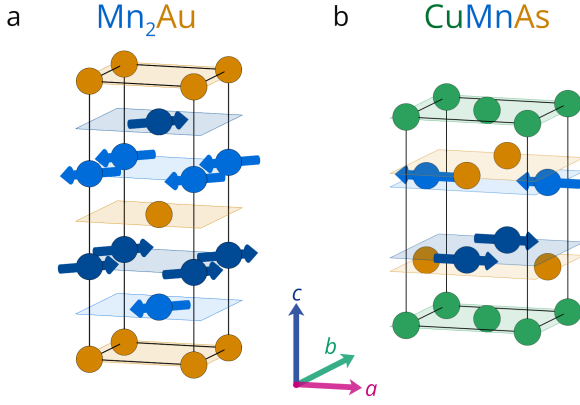


Figure 1: The crystal and magnetic structures of the tetragonal metal antiferromagnets **a** Mn_2Au and **b** CuMnAs .

linear magnetoelectric effect of the corresponding strength, is able to describe the results of the THz experiment given in Ref. [19] without involving other mechanisms of the spin dynamics excitations. Thus, we have shown that the experimental studies of antiferromagnetic Néel vector switching by the strong picosecond pulses of THz electric fields in these spintronic materials require the consideration of the magnetoelectric effect.

2. Magnetoelectric antiferromagnets

Mn_2Au and CuMnAs (orthorhombic in the bulk form and tetragonal in the thin film grown on GaAs or GaP [20]) with tetragonal crystal structures have the nonsymmorphic space groups $I4/mmm$ (#139, D_{4h}^{17}) [21] and $P4/nmm$ (#129, D_{4h}^7) [20] and four formula units per unit cell $Z = 4$, respectively. The lattice parameters at room temperature are $a = b = 3.33 \text{ \AA}$ and $c = 8.54 \text{ \AA}$ for Mn_2Au [21] and $a = b = 3.82 \text{ \AA}$ and $c = 6.32 \text{ \AA}$ for CuMnAs [22]. At room temperature both Mn_2Au ($T_N \simeq 1350$ [21]) that exceeds the temperature about 950 K at which the compound becomes structurally unstable [23]) and CuMnAs ($T_N \simeq 480$ K [22]) provide a collinear antiferromagnetic structure with ferromagnetic layers in the ab plane antiferromagnetically aligned along the c axis [21, 22]. For Mn_2Au in-plane diagonals are easy axes of magnetic anisotropy ($\mathbf{l} \parallel \langle 110 \rangle$) [21, 24] while for CuMnAs the a and b are easy axes ($\mathbf{l} \parallel \langle 100 \rangle$) [22, 25]. Besides, the energy barrier between the $\langle 110 \rangle$ and $\langle 100 \rangle$ easy axes in both compounds is small, and has a value of about $1 \mu\text{V}$ per formula unit [22, 14]. Thus, four types of different antiferromagnetic domains are expected in these materials [26]. The crystal structure and magnetic ordering of Mn_2Au and CuMnAs are shown in Fig. 1. Further we assume that $x \parallel a$, $y \parallel b$, and $c \parallel z$.

3. Magnetoelectric model

We have developed a model of magnetoelectric-driven spin dynamics near the ground state in a metallic antiferromagnet Mn_2Au only because the results for the CuMnAs will

be qualitatively similar. The magnetic moment of Mn ions is of the same value $|\mathbf{m}_1| = |\mathbf{m}_2| = |\mathbf{m}_3| = |\mathbf{m}_4| = m_0$, so it is convenient to use the two-sublattice approximation with two opposite sublattice magnetizations $\mathbf{m}_A = \frac{\mathbf{m}_1 + \mathbf{m}_3}{2m_0}$ and $\mathbf{m}_B = \frac{\mathbf{m}_2 + \mathbf{m}_4}{2m_0}$. Then we define the net magnetization vector $\mathbf{m} = \frac{\mathbf{m}_A + \mathbf{m}_B}{2}$ and antiferromagnetic vector $\mathbf{l} = \frac{\mathbf{m}_A - \mathbf{m}_B}{2}$. We use the spherical coordinate system with polar ϑ and azimuthal φ angles, where the sublattice magnetization vectors are $\mathbf{m}_{A(B)} = (\sin \vartheta_{A(B)} \cos \varphi_{A(B)}, \sin \vartheta_{A(B)} \sin \varphi_{A(B)}, \cos \vartheta_{A(B)})$. Then, \mathbf{m}_A and \mathbf{m}_B are parameterized as follows [27, 28, 29]

$$\begin{aligned} \vartheta_A &= \vartheta - \epsilon, & \vartheta_B &= \pi - \vartheta - \epsilon, \\ \varphi_A &= \varphi + \beta, & \varphi_B &= \pi + \varphi - \beta, \end{aligned} \quad (1)$$

where small canting angles $\epsilon \ll 1$ and $\beta \ll 1$ are introduced. We expand the net magnetization \mathbf{m} and antiferromagnetic \mathbf{l} vector Cartesian components in series with respect to the small canting angles ϵ and β . The resulting expressions are

$$\begin{aligned} m_x &\approx -\beta \sin \vartheta \sin \varphi - \epsilon \cos \vartheta \cos \varphi, \\ m_y &\approx \beta \sin \vartheta \cos \varphi - \epsilon \cos \vartheta \sin \varphi, \\ m_z &\approx \epsilon \sin \vartheta, \\ l_x &\approx \sin \vartheta \cos \varphi, \\ l_y &\approx \sin \vartheta \sin \varphi, \\ l_z &\approx \cos \vartheta. \end{aligned} \quad (2)$$

The magnetic moments of the Mn ions are aligned in the xy plane of Mn_2Au . The energy of the easy-plane magnetic anisotropy, taking into account Eq. (2), has the form

$$\begin{aligned} U_A &= -K_1 (l_x^2 + l_y^2) + K_2 (l_x^4 + l_y^4) \\ &\approx -K_1 \sin^2 \vartheta + K_2 \sin^4 \vartheta (\cos^4 \varphi + \sin^4 \varphi), \end{aligned} \quad (3)$$

where $K_{1,2}$ are the easy-plane magnetic anisotropy parameters. To find the ground state we minimize U_A with respect to ϑ and φ angles by solving the equations

$$\begin{aligned} \frac{\partial U_A}{\partial \vartheta} &= \left[-K_1 + 2K_2 \sin 2\vartheta (\cos^4 \varphi + \sin^4 \varphi) \right] \sin 2\vartheta = 0, \\ \frac{\partial U_A}{\partial \varphi} &= -K_2 \sin^4 \vartheta \sin 4\varphi = 0, \end{aligned} \quad (4)$$

with the assumption that $K_1 > 0$, $K_2 > 0$, and $|K_1| \gg |K_2|$ and the following conditions

$$\begin{aligned} \frac{\partial^2 U_A}{\partial \vartheta^2} &\approx -2K_1 \cos 2\vartheta > 0, \\ \frac{\partial^2 U_A}{\partial \varphi^2} &= -4K_2 \sin^4 \vartheta \cos 4\varphi > 0. \end{aligned} \quad (5)$$

Then the ground state is defined by the angles $\vartheta_0 = \frac{\pi}{2}$, and

$$\varphi_0 = \pm \frac{\pi}{4}, \pm \frac{3\pi}{4}.$$

Near the ground state the angles can be expressed as $\vartheta = \vartheta_0 + \vartheta_1$ and $\varphi = \varphi_0 + \varphi_1$, where $\vartheta_1 \ll 1$ and $\varphi_1 \ll 1$. Then, taking into account the following relations

$$\begin{aligned} \sin \vartheta &\approx 1 - \frac{\vartheta_1^2}{2}, \quad \cos \vartheta \approx -\vartheta_1, \\ \sin \varphi &\approx \left(1 - \frac{\varphi_1^2}{2}\right) \sin \varphi_0 + \varphi_1 \cos \varphi_0, \\ \cos \varphi &\approx \left(1 - \frac{\varphi_1^2}{2}\right) \cos \varphi_0 - \varphi_1 \sin \varphi_0, \end{aligned} \quad (6)$$

we can represent vector components \mathbf{m} and \mathbf{l} [Eqs. (2)] in the following form

$$\begin{aligned} m_x &\approx -\beta \sin \varphi_0, \\ m_y &\approx \beta \cos \varphi_0, \\ m_z &\approx \epsilon, \\ l_x &\approx \left(1 - \frac{\vartheta_1^2}{2} - \frac{\varphi_1^2}{2}\right) \cos \varphi_0 - \varphi_1 \sin \varphi_0, \\ l_y &\approx \left(1 - \frac{\vartheta_1^2}{2} - \frac{\varphi_1^2}{2}\right) \sin \varphi_0 + \varphi_1 \cos \varphi_0, \\ l_z &\approx -\vartheta_1. \end{aligned} \quad (7)$$

Thus, the anisotropy energy U_A (3) in the vicinity of the magnetic ground state $\varphi_0 = \frac{\pi}{4}$ up to a constant term can be represented as

$$\begin{aligned} U_A &\approx (K_1 - 2K_2 a_0) \vartheta_1^2 + K_2 a_1 \varphi_1 + K_2 a_2 \varphi_1^2 \\ &\approx (K_1 - K_2) \vartheta_1^2 + 2K_2 \varphi_1^2, \end{aligned} \quad (8)$$

where the used parameters are $a_0 = \cos^4 \varphi_0 + \sin^4 \varphi_0 = \frac{1}{2}$, $a_1 = -\sin 4\varphi_0 = 0$, $a_2 = -2 \cos^4 \varphi_0 + 12 \cos^2 \varphi_0 \sin^2 \varphi_0 - 2 \sin^4 \varphi_0 = 2$.

The kinetic energy of the spin system in a double-sublattice antiferromagnet per one magnetic ion can be determined through the Berry phase gauge $\gamma_{\text{Berry}} = (1 - \cos \vartheta_A) \dot{\varphi}_A + (1 - \cos \vartheta_B) \dot{\varphi}_B$ [30, 29] in the first order in ϵ and β as

$$T = S\hbar (\epsilon \dot{\varphi}_1 + \beta \dot{\vartheta}_1) = \frac{m_0}{\gamma} (\epsilon \dot{\varphi}_1 + \beta \dot{\vartheta}_1), \quad (9)$$

where S is the spin for magnetic ions and γ is the gyromagnetic ratio.

The exchange energy of the magnetic system in a double-sublattice antiferromagnet in the second order of ϵ and β up to a constant term can be represented as

$$U_{\text{Ex}} = \lambda_{\text{Ex}} m_0^2 \mathbf{m}_A \cdot \mathbf{m}_B \approx 2 \lambda_{\text{Ex}} m_0^2 (\epsilon^2 + \beta^2), \quad (10)$$

where λ_{Ex} is the exchange interaction constant between neighboring spins of Mn ions.

The interaction of the spin system with the external magnetic field \mathbf{H} applied in the xy plane is described by the Zee-

man term, which according to Eqs. (2) and (7) has the following form

$$\begin{aligned} U_Z &= -m_0 \mathbf{m} \cdot \mathbf{H} = -m_0 [m_x H_x + m_y H_y] \\ &\approx m_0 [\beta \sin \vartheta (\sin \varphi H_x - \cos \varphi H_y) \\ &\quad + \epsilon \cos \vartheta (\cos \varphi H_x + \sin \varphi H_y)] \\ &\approx m_0 [\beta (\sin \varphi_0 H_x - \cos \varphi_0 H_y) \\ &\quad + (\beta \varphi_1 - \epsilon \vartheta_1) (\cos \varphi_0 H_x + \sin \varphi_0 H_y)]. \end{aligned} \quad (11)$$

According to the symmetry, the magnetoelectric energy in CuMnAs and Mn₂Au has the following form

$$\begin{aligned} U_{\text{ME}} &= -\lambda_{\text{ME1}} m_0 l_z (m_x P_y + m_y P_x) - \lambda_{\text{ME2}} m_0 m_z (l_x P_y + l_y P_x) \\ &\quad - \lambda_{\text{ME3}} m_0 P_z (l_y m_x + l_x m_y), \end{aligned} \quad (12)$$

where $\lambda_{\text{ME1-3}}$ are the dimensionless magnetoelectric parameters. For simplicity, we assume that the polarization \mathbf{P} is induced by the electric field \mathbf{E} applied in the xy plane. Note that since spin dynamics will be considered, the expression for U_{ME} [Eq. (12)] is given for polarization \mathbf{P} , which is a dynamical variable, and not for the electric field \mathbf{E} , which is an external influence in this case [8]. Then, taking into account Eq. (7) and neglecting small angles above the second order, Eq. (12) near the ground state has the form

$$\begin{aligned} U_{\text{ME}} &= -\lambda_{\text{ME1}} m_0 l_z (m_x P_y + m_y P_x) - \lambda_{\text{ME2}} m_0 m_z (l_x P_y + l_y P_x) \\ &\approx \lambda_{\text{ME1}} m_0 \beta \frac{\sin 2\vartheta}{2} (\sin \varphi P_y - \cos \varphi P_x) \\ &\quad + \epsilon m_0 (\lambda_{\text{ME1}} \cos^2 \vartheta - \lambda_{\text{ME2}} \sin^2 \vartheta) (\cos \varphi P_y + \sin \varphi P_x) \\ &\approx m_0 (\lambda_{\text{ME2}} \epsilon \varphi_1 - \lambda_{\text{ME1}} \beta \vartheta_1) (\sin \varphi_0 P_y - \cos \varphi_0 P_x) \\ &\quad - \lambda_{\text{ME2}} m_0 \epsilon (\cos \varphi_0 P_y + \sin \varphi_0 P_x). \end{aligned} \quad (13)$$

To reveal the spin dynamics induced by the electric and magnetic fields we construct a Lagrangian \mathcal{L} general expressions for the exchange U_{Ex} (10), anisotropy U_A (3), magnetoelectric U_{ME} (13) energies and expression for the kinetic energy T close to Eq. (9)

$$\begin{aligned} \mathcal{L} &= T - U_{\text{Ex}} - U_A - U_Z - U_{\text{ME}} = \\ &= \frac{m_0}{\gamma} (\epsilon \dot{\varphi} + \beta \dot{\vartheta}) - 2\lambda_{\text{Ex}} m_0^2 (\epsilon^2 + \beta^2) \\ &\quad + K_1 \sin^2 \vartheta - K_2 \sin^4 \vartheta (\cos^4 \varphi + \sin^4 \varphi) \\ &\quad - m_0 [\beta \sin \vartheta (\sin \varphi H_x - \cos \varphi H_y) \\ &\quad + \epsilon \cos \vartheta (\cos \varphi H_x + \sin \varphi H_y)] \\ &\quad - \lambda_{\text{ME1}} m_0 \beta \frac{\sin 2\vartheta}{2} (\sin \varphi P_y - \cos \varphi P_x) \\ &\quad - \epsilon m_0 (\lambda_{\text{ME1}} \cos^2 \vartheta - \lambda_{\text{ME2}} \sin^2 \vartheta) (\cos \varphi P_y + \sin \varphi P_x). \end{aligned} \quad (14)$$

The Rayleigh dissipation function is [7]

$$\mathcal{R} = \frac{\alpha_G m_0}{2\gamma} \dot{\mathbf{l}}^2 = \frac{\alpha_G m_0}{2\gamma} (\dot{\vartheta}^2 + \dot{\varphi}^2 \sin^2 \vartheta), \quad (15)$$

where α_G is the Gilbert damping constant. Note that all terms in Eq. (14) are considered for a single molecule units. Then we substitute the Lagrangian (14) and Rayleigh dissipation function (15) into the Euler-Lagrange equations

$$\frac{d}{dt} \frac{\partial \mathcal{L}}{\partial \dot{q}_i} - \frac{\partial \mathcal{L}}{\partial q_i} = -\frac{\partial \mathcal{R}}{\partial \dot{q}_i}, \quad (16)$$

where q_i for $i = 1-4$ are order parameters ϵ , φ , β , and ϑ , respectively. As a result, we obtain a system of four differential equations describing the spin dynamics of the magnetoelectric antiferromagnet induced by the electric and magnetic fields

$$\begin{aligned} \dot{\epsilon} - \frac{\omega_{A2}}{4} \sin^4 \vartheta \sin 4\varphi + \frac{2}{\tau_M \omega_{Ex}} \dot{\varphi} \sin^2 \vartheta \\ + \gamma \lambda_{ME1} \beta \frac{\sin 2\vartheta}{2} (\cos \varphi P_y + \sin \varphi P_x) \\ + \epsilon \gamma (\lambda_{ME1} \cos^2 \vartheta - \lambda_{ME2} \sin^2 \vartheta) (\cos \varphi P_x - \sin \varphi P_y) \\ = -\gamma [\beta \sin \vartheta (\cos \varphi H_x + \sin \varphi H_y) \\ + \epsilon \cos \vartheta (\cos \varphi H_y - \sin \varphi H_x)], \\ \dot{\varphi} - \omega_{Ex} \epsilon - \gamma (\lambda_{ME1} \cos^2 \vartheta - \lambda_{ME2} \sin^2 \vartheta) \\ (\cos \varphi P_y + \sin \varphi P_x) = \gamma \cos \vartheta (\cos \varphi H_x + \sin \varphi H_y), \\ \dot{\beta} - \frac{\omega_{A1}}{2} \sin 2\vartheta + \omega_{A2} \sin^2 \vartheta \frac{\sin 2\vartheta}{2} (\cos^4 \varphi + \sin^4 \varphi) \\ + \frac{2}{\tau_M \omega_{Ex}} \dot{\vartheta} + \gamma \lambda_{ME1} \beta \cos 2\vartheta (\sin \varphi P_y - \cos \varphi P_x) \\ - \epsilon \gamma \sin 2\vartheta (\lambda_{ME1} + \lambda_{ME2}) (\cos \varphi P_y + \sin \varphi P_x) \\ = -\gamma [\beta \cos \vartheta (\sin \varphi H_x - \cos \varphi H_y) \\ - \epsilon \sin \vartheta (\cos \varphi H_x + \sin \varphi H_y)], \\ \dot{\vartheta} - \omega_{Ex} \beta - \gamma \lambda_{ME1} \frac{\sin 2\vartheta}{2} (\sin \varphi P_y - \cos \varphi P_x) \\ = \gamma \sin \vartheta (\sin \varphi H_x - \cos \varphi H_y), \end{aligned} \quad (17)$$

where the used parameters are $\omega_{A1} = 2\gamma K_1/m_0 = \gamma H_{A1}$, $\omega_{A2} = 4\gamma K_2/m_0 = \gamma H_{A2}$, $\omega_{Ex} = 4\gamma \lambda_{Ex} m_0 = \gamma H_{Ex}$, and $\tau_M = 2/(\alpha_G \omega_{Ex}) = 3.33$ ps is the magnon damping time from Ref. [19], that we introduced into the system of differential equations.

Near the ground state the Lagrangian (14) is linearized and takes a simplified form

$$\begin{aligned} \mathcal{L} = T - U_{Ex} - U_A - U_Z - U_{ME} = \\ \frac{m_0}{\gamma} (\epsilon \dot{\varphi}_1 + \beta \dot{\vartheta}_1) - 2 \lambda_{Ex} m_0^2 (\epsilon^2 + \beta^2) \\ - (K_1 - K_2) \vartheta_1^2 - 2 K_2 \varphi_1^2 \\ - m_0 [\beta (\sin \varphi_0 H_x - \cos \varphi_0 H_y) \\ + (\beta \varphi_1 - \epsilon \vartheta_1) (\cos \varphi_0 H_x + \sin \varphi_0 H_y)] \\ - m_0 (\lambda_{ME2} \epsilon \varphi_1 - \lambda_{ME1} \beta \vartheta_1) (\sin \varphi_0 P_y - \cos \varphi_0 P_x) \\ + \lambda_{ME2} m_0 \epsilon (\cos \varphi_0 P_y + \sin \varphi_0 P_x), \end{aligned} \quad (18)$$

substituting which into the Euler-Lagrange equations (16) with the Rayleigh dissipation function (15) we obtain a sys-

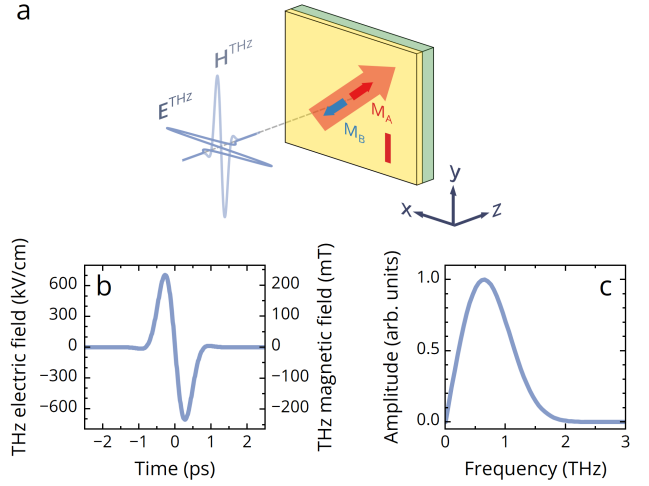


Figure 2: a Schematic of simulated experiment for studying of the THz driven spin dynamics in an antiferromagnetic thin film. b Terahertz pulse waveform and c corresponding normalized Fourier spectrum.

tem of four linearized differential equations of the spin dynamics

$$\begin{aligned} \dot{\epsilon} + \omega_{A2} \varphi_1 + \frac{2}{\tau_M \omega_{Ex}} \dot{\varphi}_1 + \gamma \lambda_{ME2} \epsilon (\sin \varphi_0 P_y - \cos \varphi_0 P_x) \\ = -\gamma \beta (\cos \varphi_0 H_x + \sin \varphi_0 H_y), \\ \dot{\varphi}_1 - \omega_{Ex} \epsilon - \gamma \lambda_{ME2} \varphi_1 (\sin \varphi_0 P_y - \cos \varphi_0 P_x) \\ = -\gamma \vartheta_1 (\cos \varphi_0 H_x + \sin \varphi_0 H_y) - \gamma \lambda_{ME2} (\cos \varphi_0 P_y + \sin \varphi_0 P_x), \\ \dot{\beta} + (\omega_{A1} - \frac{\omega_{A2}}{2}) \vartheta_1 + \frac{2}{\tau_M \omega_{Ex}} \dot{\vartheta}_1 - \gamma \lambda_{ME1} \beta (\sin \varphi_0 P_y - \cos \varphi_0 P_x) \\ = \gamma \epsilon (\cos \varphi_0 H_x + \sin \varphi_0 H_y), \\ \dot{\vartheta}_1 - \omega_{Ex} \beta + \gamma \lambda_{ME1} \vartheta_1 (\sin \varphi_0 P_y - \cos \varphi_0 P_x) \\ = \gamma [(\sin \varphi_0 H_x - \cos \varphi_0 H_y) + \varphi_1 (\cos \varphi_0 H_x + \sin \varphi_0 H_y)]. \end{aligned} \quad (19)$$

4. THz driven spin dynamics

The THz electric and magnetic field pulses are effective stimuli for the excitation of spin dynamics in antiferromagnets [1, 31, 32, 33]. To simulate the THz driven spin dynamics experiment (see Fig. 2a), we solve the Eq. (17) with a near single-cycle THz pulse given by the Gaussian function for the THz electric field

$$E_0^{THz}(t) = -E_0 \exp\left(-\frac{t^2}{\tau_{THz}^2}\right) \sin \omega_{THz} t, \quad (20)$$

where E_0 is the peak electric field strength, τ_{THz} and ω_{THz} determine the THz pulse duration and frequency, respectively. The THz magnetic field is related to the THz electric field as $|H_0^{THz}(t)| = |E_0^{THz}(t)|$ in Gaussian units. For the THz pulse propagating along the z axis the electric and magnetic field strength vectors are defined as $\mathbf{E}_0^{THz} = E_0^{THz}(t)(\cos \alpha, \sin \alpha, 0)$

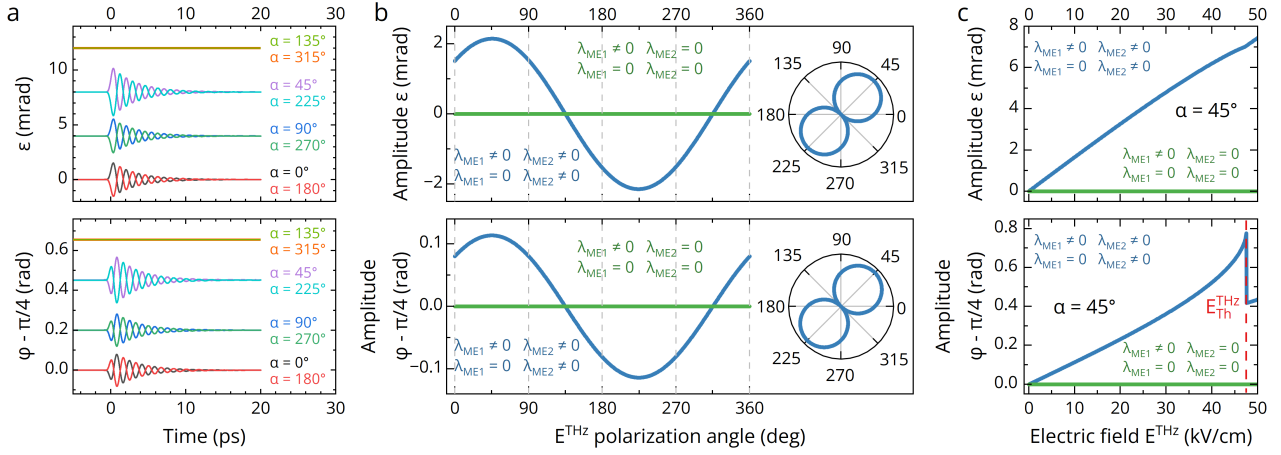


Figure 3: Spin dynamics induced by the THz pump pulses in a single antiferromagnetic domain with $\varphi_0 = \pi/4$. **a** Transients of the $\epsilon(t)$ (upper frame) and $\varphi(t)$ (lower frame) for different THz pump polarization angles α with respect to the x axis. **b** The signed Fourier amplitude of oscillations $\epsilon(t)$ (upper frame) and $\varphi(t)$ (lower frame) as a function of the THz pump polarization angle α obtained for various parameters λ_{ME1} and λ_{ME2} of Eq. (17). The sign change corresponds to the π shift of oscillation phases. Insets show the same in polar diagrams. **c** Dependence of amplitude of oscillations $\epsilon(t)$ (upper frame) and $\varphi(t)$ (lower frame) on the THz electric field strength E^{THz} inside film obtained with polarization angle α for various parameters λ_{ME1} and λ_{ME2} of Eq. (17). The $E_{\text{Th}}^{\text{THz}}$ is a threshold strength of the THz electric field at exceeding of which switching of antiferromagnetic Néel vector \mathbf{l} occurs.

and $\mathbf{H}^{\text{THz}} = H^{\text{THz}}(t)(-\sin \alpha, \cos \alpha, 0)$, where α is the polarization angle with respect to the x axis. Note that $\mathbf{E}_0^{\text{THz}}$ and $\mathbf{H}_0^{\text{THz}}$ are perpendicular to each other. The THz pulse parameters from Eq. (20) were taken close to the experimental one with peak electric field strength 760 kV/cm and corresponding magnetic field 250 mT, with a pulse duration about 2 ps and maximum on the spectra at the 0.6 THz as shown in Fig. 2b and 2c. The emerging spin response can be detected experimentally using femtosecond magneto-optic probes [3].

It is well known that the tangential component of the strength of the THz electric field \mathbf{E}^{THz} on the surface with infinite conductivity is zero [34]. In the surface with finite but good conductivity and thickness larger than the spin depth, the tangential component of \mathbf{E}^{THz} obeys the Leontovich bound-

ary condition $\mathbf{E}^{\text{THz}} = Z_S \mathbf{H}^{\text{THz}}$, where $Z_S = \sqrt{\frac{\mu \omega_{\text{THz}}}{2\sigma}}$ is

the effective surface impedance and μ is the magnetic permeability of free space [34]. In our case, we assume that the thickness d of the metallic film with a typical conductivity about $\sigma \simeq 1.5 \times 10^6$ S/m [19] is significantly less than the

skin depth $\delta = \sqrt{\frac{2}{\omega \mu \sigma}} \simeq 410$ nm [18, 19] and the THz

electric field can be considered to be homogeneous across the thickness. Then, the THz electric field in the metallic film can be estimated using the Fresnel equation for normal incidence, when the amplitude of the transmission t_{film} through the interface between air ($n_{\text{air}} \simeq 1$) and substrate ($n_{\text{sub}} \simeq 3$) with thin ($d \simeq 50$ nm) metallic film is considered [35, 19]

$$t_{\text{film}} = \frac{2n_{\text{air}}}{n_{\text{air}} + n_{\text{sub}} + Z_0 \sigma d}, \quad (21)$$

where $Z_0 \simeq 376.7$ Ohm is the impedance of free space. We can assume that the THz electric field at this interface is equal to the THz electric field inside the thin metallic film $E^{\text{THz}} = t_{\text{film}} E_0^{\text{THz}}$. For the metallic film parameters we used, the amplitude of transmission t_{film} is 6.2×10^{-2} , which means that the THz electric field in the metal film E^{THz} does not exceed the value of about 47 kV/cm for our single-cycle THz pulse.

In metals, an applied electric field \mathbf{E} induces an electric current with density \mathbf{J} , the relationship between which obeys Ohm's law $\mathbf{J} = \sigma \mathbf{E}$. The electric current density \mathbf{J} is also related to the polarization \mathbf{P} change through its time derivative $\mathbf{J} = \dot{\mathbf{P}}$. Hence, the induced polarization \mathbf{P}^{THz} in metals is related to the THz electric field \mathbf{E}^{THz} by the following relation

$$\mathbf{P}^{\text{THz}}(t) = \sigma \int_{-\infty}^t \mathbf{E}^{\text{THz}}(t') dt'. \quad (22)$$

We assume that the conductivity of the metallic film σ is constant in the frequency range of our THz pulse. Therefore, using Eqs. (22) and (21) we can estimate the polarization \mathbf{P}^{THz} in a thin metallic film induced by the THz electric field $\mathbf{E}_0^{\text{THz}}$ given by Eq. (20).

Next we need to determine the values of the parameters included in the system of Eqs. (17). According to the literature for CuMnAs [36], the exchange field is about $H_{\text{Ex}} = \omega_{\text{Ex}}/\gamma \simeq 7 \times 10^6$ Oe, the anisotropy field is about $H_{A2} = \omega_{A2}/\gamma \simeq 50$ Oe. These values allow us to estimate the frequency of the antiferromagnetic resonance for CuMnAs as $\omega_M = \sqrt{\omega_{\text{Ex}} \omega_{A2}} = \gamma \sqrt{H_{\text{Ex}} H_{A2}} \simeq 50$ GHz. For Mn₂Au the exchange field is estimated as $H_{\text{Ex}} = \omega_{\text{Ex}}/\gamma \simeq 1.3 \times 10^7$ Oe [21], while there is no common agreement in the literature on the antiferromagnetic resonance frequency. The

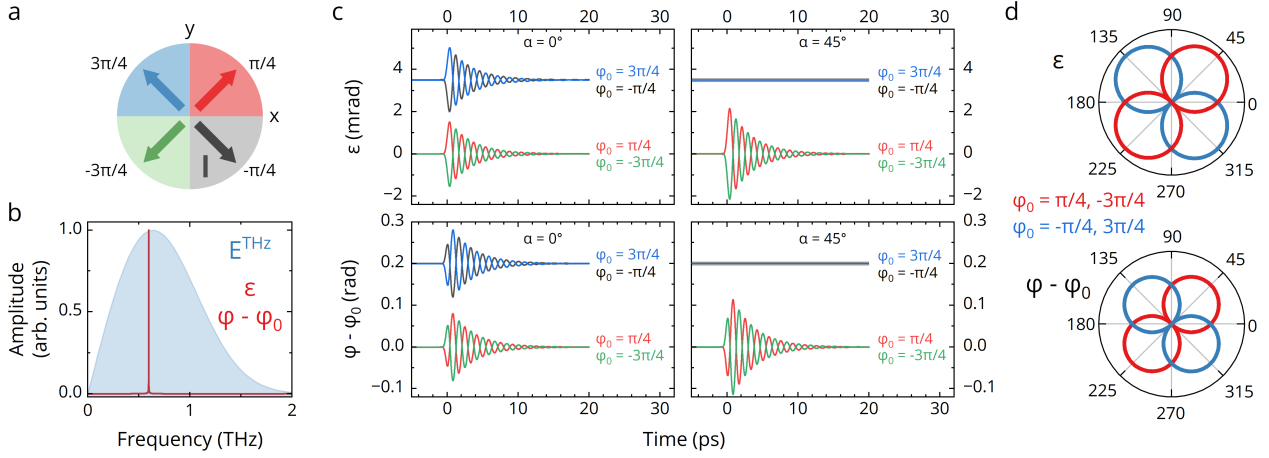


Figure 4: Spin dynamics induced by the THz electric field E^{THz} in four antiferromagnetic domains with $\varphi_0 = \pi/4, -\pi/4, 3\pi/4, 3\pi/4$ schematically shown in **a**. **b** Fourier spectra of the oscillations $\epsilon(t)$ and $\varphi(t)$ with a resonance at 0.6 THz induced by the THz pump pulse. The spectra of the THz pump pulse is shown by the blue area. **c** Transients of the $\epsilon(t)$ (upper frames) and $\varphi(t)$ (lower frames) induced by the THz pump with polarization angles $\alpha = 0^\circ$ (left frames) and 45° (right frames) for four antiferromagnetic domains. **d** The polar diagrams of the amplitude of oscillations $\epsilon(t)$ (upper frame) and $\varphi(t)$ (lower frame) as a function of the THz pump polarization angle α in four antiferromagnetic domains.

Raman scattering gives the value of $\omega_M \simeq 120$ GHz, that corresponds to the anisotropy field of $H_{A2} = \omega_{A2}/\gamma \simeq 140$ Oe [37]. On the other hand, recent pump-probe experiments give $\omega_M \simeq 0.6$ THz that corresponds to the anisotropy field $H_{A2} \simeq 3500$ Oe [19] that we will be using in our numerical simulations. We note that this frequency is resonant with the THz pump pulse used by us. The net magnetization of the antiferromagnetic sublattice per unit volume can be estimated as $m_0 = \mu_{\text{Mn}} N_{\text{Mn}} \simeq 780$ Oe, where $N_{\text{Mn}} \simeq 2.1 \times 10^{22} \text{ cm}^{-3}$ is the number of Mn ions in one antiferromagnetic sublattice per unit volume and $\mu_{\text{Mn}} \simeq 4\mu_B$ is the Mn magnetic moment [21]. Thus, we can evaluate the

exchange interaction constant $\lambda_{\text{Ex}} = \frac{H_{\text{Ex}}}{4m_0} \simeq 4.2 \times 10^3$ and

the perpendicular susceptibility $\chi_{\perp} = 1/\lambda_{\text{Ex}} \simeq 2.4 \times 10^{-4}$ which is close to the experimental value 7.5×10^{-4} from Ref. [21]. The anisotropy field $H_{A1} \simeq 10^5$ Oe [38, 39] which is significantly larger than $H_{A1} \gg H_{A2}$ [39, 21, 37] was employed to simulate the spin dynamics in both materials. Taking this into account and assuming that there is no significant difference in the magnetoelectric parameters λ_{ME2} and λ_{ME3} in Eq. (12), as in the case of Cr_2O_3 , we focus in the study of spin dynamics in Mn_2Au in the xy plane since the smaller THz electric fields are required compared to the electric field needed to induce spin dynamics in other planes.

The values of magnetoelectric susceptibilities for metallic antiferromagnets CuMnAs and Mn_2Au are not available in the literature [6] to the best of our knowledge. However, the Ref. [19] provides experimental results on THz driven spin dynamics in Mn_2Au in the geometry that we use in Fig. 2a. Assuming that the main excitation mechanism in this case is the linear magnetoelectric effect and neglecting the other effects, we can estimate the dimensionless magnetoelectric parameters $\lambda_{\text{ME1-2}}$ from the simulation of these experimental results.

We performed simulations of the THz driven spin dynamics in Mn_2Au solving the system of Eqs. (17) with the THz pump pulse described by Eq. (20). We employed the THz electric field with strength $E^{\text{THz}} \simeq 10$ kV/cm inside the film which corresponds to the incident field about $E_0^{\text{THz}} \simeq 160$ kV/cm wherever not otherwise specified. For the CuMnAs , the solved spin dynamics are qualitatively the same, but differ in magnitude. It is worth noting that we focus on studying the spin dynamics in the xy plane, which is described by the ϵ and φ variables in Eq. (17). Figure 3a shows the transients of the $\epsilon(t)$ and $\varphi(t)$ for different THz pump polarization angles α for a single antiferromagnetic domain with $\varphi_0 = \pi/4$ and previously defined parameters. To gain further insights, we estimated the dependence of the signed Fourier amplitude of the oscillations of $\epsilon(t)$ and $\varphi(t)$ on the THz pump polarization angle α . The sign of the amplitude is related to the π shift of the oscillation phases. Moreover, the most pronounced oscillations of ϵ and φ angles are observed at polarization of the THz pump E^{THz} along the antiferromagnetic Néel vector \mathbf{I} at $\alpha = 45^\circ$ and 225° , while the spin dynamics is not excited when E^{THz} and \mathbf{I} are mutually perpendicular at $\alpha = 135^\circ$ and 315° (see Figs. 3a–3b).

The amplitude of oscillations of ϵ and φ have close to linearly dependences on the THz electric field strength inside film E^{THz} up to about 30 kV/cm after which these dependences become significantly nonlinear due to nonlinear spin dynamics from Eq. (17). Note that the close to linear THz electric field dependence of φ is consistent with experimental findings from Ref. [19]. The THz electric field polarization reversal causes a π shift of the oscillation phases. These observations are consistent with the experimental results from Ref. [19] where the THz pump pulse polarized along the antiferromagnetic Néel vector \mathbf{I} with a strength of electric field estimated as 40 kV/cm on the surface of the metallic film excited a maximum deflection of the ϕ about

0.5 rad (30°). The comparison of the simulations with these experimental results allowed us to estimate the magnetoelectric parameter $\lambda_{\text{ME2}} \simeq 0.1$ which corresponds to the dimensionless magnetoelectric susceptibility $\alpha_{\text{ME2}} = \lambda_{\text{ME2}} \chi_{\perp} / \sqrt{2} \simeq 2 \times 10^{-5}$ for Mn_2Au . This value is about an order of magnitude smaller than the value of the magnetoelectric response in prototypical antiferromagnet Cr_2O_3 [40, 41, 42, 8] and many orders of magnitude less than the record values reported in DyFeO_3 [43, 44] and in other known magnetoelectrics such as TbPO_4 [44] and LiCoPO_4 [9, 45].

Next, we revealed the effects of the magnetoelectric parameters λ_{ME1} and λ_{ME2} and Zeeman torque on the oscillations of $\epsilon(t)$ and $\varphi(t)$, taking and not taking them into account when solving Eq. (17). We performed simulations of spin dynamics for two cases with $\lambda_{\text{ME1}} \neq 0$, $\lambda_{\text{ME2}} \neq 0$ and $\lambda_{\text{ME1}} = 0$, $\lambda_{\text{ME2}} \neq 0$ and we did not reveal any significant differences as shown by blue lines in Figs. 3(b) and 3(c). Besides, there is no significant spin dynamics at $\lambda_{\text{ME2}} = 0$ as seen by green lines in Figs. 3(b) and 3(c). Thus, at the employed strength of the THz pump electric field, the THz driven spin dynamics described by $\epsilon(t)$ and $\varphi(t)$ is defined by the magnetoelectric parameter λ_{ME2} , whereas the parameter λ_{ME1} and Zeeman torque can be neglected. This is due to that the Zeeman torque drives the out-of-plane magnon with a frequency much higher than ω_{M} because $H_{\text{A1}} \gg H_{\text{A2}}$.

Let us discuss the features of THz driven spin dynamics in four antiferromagnetic domains in which \mathbf{l} has an angle $\varphi_0 = \pm\pi/4, \pm 3\pi/4$ with respect to the x axis, as sketched in Fig. 4(a). For this, we numerically solve Eq. (17) varying the initial conditions for $\varphi(t)$ with the previously defined parameters of Mn_2Au and the THz pump pulse. Note that the frequency of oscillations for $\epsilon(t)$ and $\varphi(t)$ is 0.6 THz which coincides with the maximum of the THz pump spectrum [see Fig. 4(b)]. When the THz pump is linearly polarized at $\alpha = 0^\circ$, i.e., along the x axis, we observe oscillations of the $\epsilon(t)$ and $\varphi(t)$ with equal amplitudes in all antiferromagnetic domains, as shown in the left panels of Fig. 4(c). It is seen that the antiferromagnetic vector \mathbf{l} reversal leads to a π phase shift in oscillations which was also observed for φ angle in the experiment [19]. Besides, when the pump is polarized perpendicular to the antiferromagnetic vector \mathbf{l} , the spin dynamics is not excited, as shown in the right panel in Fig. 4(b). In the polar diagram of the amplitudes of oscillations for $\epsilon(t)$ and $\varphi(t)$ with respect to the THz pump polarization angle α , it is seen that in $\pi/2$ different antiferromagnetic domains the figure eight is rotated by 90° [see Fig. 4(c)]. Therefore, we have predicted that the THz electric field driven spin dynamics in Mn_2Au has features at the crossing from one antiferromagnetic domain to another.

It was previously shown that magnetoelectric driven spin dynamics can be fairly described by considering only parameter λ_{ME2} , which allows us to significantly simplify the system of differential equations (17). Near the ground state at the polar angle $\vartheta \simeq \pi/2$ and taking into account the smallness of ϵ and β angles, the first two differential equations from Eq. (17) can be reduced to a next second order differ-

ential equation

$$\ddot{\varphi} + \frac{2}{\tau_{\text{M}}} \dot{\varphi} - \frac{\omega_{\text{Ex}} \omega_{\text{A2}}}{4} \sin 4\varphi = -\gamma \lambda_{\text{ME2}} (\cos \varphi \dot{P}_y + \sin \varphi \dot{P}_x). \quad (23)$$

It is worth noting that the terms quadratically dependent on the polarization are neglected from Eq. (23) because they do not significantly affect the resulting $\varphi(t)$ in the THz electric field range of our interest. An important consequence of Eq. (23) is that it shows that the magnetoelectric torque in metallic magnetoelectrics is proportional to the time derivative of the induced polarization ($\propto \dot{\mathbf{P}}$). Here one can observe a complete analogy with a Zeeman torque in collinear antiferromagnets where spin dynamics is driven by the time derivative of the effective magnetic field ($\propto \dot{\mathbf{H}}$) [27, 46, 47, 48].

Further, if we consider the relationship between polarization \mathbf{P}^{THz} and THz electric field \mathbf{E}^{THz} [Eq. (22)] then Eq. (24) takes the form

$$\ddot{\varphi} + \frac{2}{\tau_{\text{M}}} \dot{\varphi} - \frac{\omega_{\text{Ex}} \omega_{\text{A2}}}{4} \sin 4\varphi = -\gamma \sigma \lambda_{\text{ME2}} (\cos \varphi E_y + \sin \varphi E_x). \quad (24)$$

This Eq. (24) is similar to the equation for spin dynamics driven by the Néel spin-orbit torque from Ref. [19]. In both cases the torque is proportional to the product of the conductivity σ by the THz electric field E^{THz} inside the metallic film and distinguished only in the definition of the coefficients. The linear magnetoelectric effect analyzed in this work is qualitatively similar to the Néel spin-orbit torque discussed in Ref. [19]. In the both cases, the THz electric field results in an out-of-plane magnetization m_z which is followed by dynamics of the antiferromagnetic Néel vector \mathbf{l} in the same xy plane. The Néel spin-orbit torque arises from the THz electric field which leads to staggered spin-orbit fields acting on opposite magnetic sublattices [19]. The linear magnetoelectric effect resulting from the symmetry allowed term $\lambda_{\text{ME2}} m_0 m_z (l_x E_y + l_y E_x)$ from Eq. (12). The both effects require antiferromagnets with broken inversion symmetry and strong spin-orbit coupling [49, 50, 6]. Hence, qualitatively our simulation results must be also in agreement with the experimental observations for THz driven spin dynamics in Mn_2Au from Ref. [19]. It is important to mention once again that, there is absolutely no data on magnetoelectric susceptibilities α_{ME} in Mn_2Au and in our simulations we assumed the dimensionless magnetoelectric parameter λ_{ME2} that allows us to describe the main experimental results from Ref. [19]. Also, the value of the Néel spin-orbit torque in Mn_2Au at THz frequencies is not known. Hence, any quantitative comparison of the experimental results from Ref. [19] either with our simulations or with simulations from Ref. [19] is difficult. Moreover, unambiguous identification of the physical mechanism of the THz-driven spin dynamics in these materials requires further research.

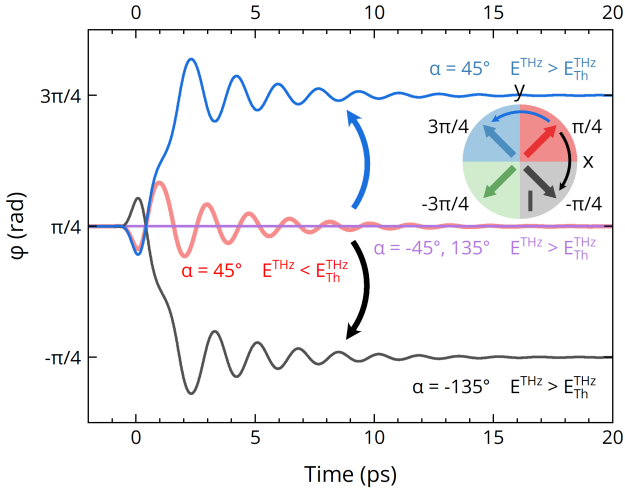


Figure 5: Switching of the antiferromagnetic vector \mathbf{I} from ground state with $\varphi_0 = \pi/4$ (red curve) to ones with $3\pi/4$ (blue curve) and $-\pi/4$ (black curve) under the THz pump pulse with electric field strength over the threshold value $E^{\text{THz}} > E_{\text{Th}}^{\text{THz}}$ and linear polarization at the angles 45° and -135° , respectively. No switching is observed under the THz pump with linear polarization at the angles -45° and 135° (purple curve). Inset schematically shows the switching of the antiferromagnetic Néel vector \mathbf{I} .

5. Spin switching

Now, we consider the switching of the antiferromagnetic vector \mathbf{I} by an applied THz electric field in Mn_2Au . Numerically solving the system of Eq. (17) varying the THz electric field strength, we observed the switching of the antiferromagnetic vector \mathbf{I} from $\varphi_0 = \pi/4$ to another ground state when the field strength exceeds the threshold $E^{\text{THz}} > E_{\text{Th}}^{\text{THz}} \simeq 47.5 \text{ kV/cm}$ inside the metallic film (see Fig. 3c), that corresponds to the incident field of about 766 kV/cm . We note that the obtained threshold THz electric field $E_{\text{Th}}^{\text{THz}}$ is about two times less than the estimate given in Ref. [19], which presumably is due to the difference in the shape of the THz pulse and the way in which it is taken into account in the equation. By control of the THz polarization angle α we can manipulate the final state of the antiferromagnetic Néel vector \mathbf{I} after switching. When the THz pulse is polarized at the $\alpha = 45^\circ$ with respect to the x axis, i.e., parallel to the antiferromagnetic vector \mathbf{I} , the switching occurs from $\varphi_0 = \pi/4$ to $-\pi/4$, while at $\alpha = -135^\circ$, i.e., antiparallel \mathbf{I} , the final state is already $3\pi/4$, as shown in Fig. 5. Note that the THz electric field up to $E_0^{\text{THz}} \simeq 1 \text{ MV/cm}$ is available for tabletop setups with THz pulses generated by the tilted-front optical rectification of laser pulses in LiNbO_3 prism [33]. On the other hand, as mentioned previously, the values of the dimensionless magnetoelectric susceptibilities α_{ME} for Mn_2Au are missing in the literature. Therefore, if the value of α_{ME} is about 2×10^{-5} , which, however, which is a rather modest value for the linear magnetoelectric response, the switching of the antiferromagnetic Néel vector \mathbf{I} is probably possible with THz electric fields achievable in

the tabletop setups.

6. Conclusions

In summary, we have discussed the spin dynamics driven by THz electric field pulses in the metallic magnetoelectric antiferromagnetic CuMnAs and Mn_2Au thin films. We obtained the equations for spin dynamics and theoretically demonstrated that in the metallic antiferromagnetic magnetoelectrics the THz magnetoelectric torque is proportional to the time derivative of the induced polarization. By analyzing these equations it has been theoretically revealed that single-cycle THz pulses are able to induce the dynamics of the antiferromagnetic vector \mathbf{I} and its features in different antiferromagnetic domains are predicted. We have shown that our model is able to fairly describe the existing experimental results on the THz driven spin dynamics in the metallic Mn_2Au thin film from Ref. [19] by taking into account only the linear magnetoelectric effect and not considering other mechanisms.

Thus, we have demonstrated that the linear magnetoelectric effect should be taken into consideration when discussing the THz induced spin dynamics in metallic antiferromagnetic CuMnAs and Mn_2Au thin films. Moreover, it has been predicted that coherent switching of the antiferromagnetic Néel vector \mathbf{I} from one to another ground state caused by the magnetoelectric effect occurs when the THz electric field with linear polarization collinear to the antiferromagnetic vector \mathbf{I} exceeds the threshold strength. For our assumed magnetoelectric susceptibility in Mn_2Au of about $\alpha_{\text{ME}} \simeq 2 \times 10^{-5}$, the measured value of which is lacking in the literature, we reveal that the threshold THz electric field inside the metallic films is about 47.5 kV/cm , which corresponds to the incident THz pump pulse with experimentally available strength about 766 kV/cm . We hope that our results will stimulate further study of THz magnetoelectric [51, 52] and novel altermagnetoelectric [53] effects in magnetic materials, which open up the prospects for future high-speed antiferromagnetic and altermagnetic memory devices.

Declaration of competing interest

The authors declare that they have no known competing financial interests or personal relationships that could have appeared to influence the work reported in this paper. The authors declare that this work has been published as a result of peer-to-peer scientific collaboration between researchers. The provided affiliations represent the actual addresses of the authors in agreement with their digital identifier (ORCID) and cannot be considered as a formal collaboration between the aforementioned institutions.

Acknowledgements

R. M. D. acknowledges support from the Russian Science Foundation under Grant No. 24-72-00106. A. K. Z. acknowledges support from the Russian Science Foundation

under Grant No. 22-12-00367. A. V. K. acknowledges support from the European Research Council ERC Grant Agreement No. 101054664 (SPARTACUS).

CRedit authorship contribution statement

R. M. Dubrovin: Data curation, Formal analysis, Funding acquisition, Investigation, Visualization, Writing - Original Draft, Writing - review & editing. **A. V. Kimel:** Conceptualization, Supervision, Writing - review & editing. **A. K. Zvezdin:** Conceptualization, Formal analysis, Funding acquisition, Investigation, Methodology, Project administration, Supervision, Validation, Writing - review & editing.

References

- [1] J. Han, R. Cheng, L. Liu, H. Ohno, S. Fukami, Coherent antiferromagnetic spintronics, *Nat. Mater.* 22 (6) (2023) 684–695. doi:10.1038/s41563-023-01492-6. URL <https://doi.org/10.1038/s41563-023-01492-6>
- [2] A. V. Kimel, A. M. Kalashnikova, A. Pogrebna, A. K. Zvezdin, Fundamentals and perspectives of ultrafast photoferroic recording, *Phys. Rep.* 852 (2020) 1–46. doi:10.1016/j.physrep.2020.01.004. URL <https://doi.org/10.1016/j.physrep.2020.01.004>
- [3] P. Němec, M. Fiebig, T. Kampfrath, A. V. Kimel, Antiferromagnetic opto-spintronics, *Nat. Phys.* 14 (3) (2018) 229–241. doi:10.1038/s41567-018-0051-x. URL <https://doi.org/10.1038/s41567-018-0051-x>
- [4] V. Baltz, A. Manchon, M. Tsai, T. Moriyama, T. Ono, Y. Tserkovnyak, Antiferromagnetic spintronics, *Rev. Mod. Phys.* 90 (2018) 015005. doi:10.1103/RevModPhys.90.015005. URL <https://link.aps.org/doi/10.1103/RevModPhys.90.015005>
- [5] T. Jungwirth, X. Marti, P. Wadley, J. Wunderlich, Antiferromagnetic spintronics, *Nat. Nanotech.* 11 (3) (2016) 231–241. doi:10.1038/nnano.2016.18. URL <https://doi.org/10.1038/nnano.2016.18>
- [6] F. Thöle, A. Keliri, N. A. Spaldin, Concepts from the linear magnetoelectric effect that might be useful for antiferromagnetic spintronics, *J. Appl. Phys.* 127 (21) (2020). doi:10.1063/5.0006071. URL <https://doi.org/10.1063/5.0006071>
- [7] A. K. Zvezdin, Z. V. Gareeva, Symmetry analysis of conductive antiferromagnetic materials CuMnAs, Mn₂Au, *Phys. Solid State* 66 (6) (1997) 784–787. doi:10.61011/PSS.2024.06.58685.42HH.
- [8] E. A. Turov, A. V. Kolchanov, V. V. Menshenin, I. F. Mirsaev, V. V. Nikolaev, Symmetry and Physical Properties of Antiferromagnets, Fizmatlit, Moscow (2001).
- [9] M. Fiebig, Revival of the magnetoelectric effect, *J. Phys. D* 38 (8) (2005) R123. doi:10.1088/0022-3727/38/8/R01. URL <https://doi.org/10.1088/0022-3727/38/8/R01>
- [10] M. Mostovoy, Multiferroics: different routes to magnetoelectric coupling, *npj Spintronics* 2 (1) (2024) 18. doi:10.1038/s44306-024-00021-8. URL <https://doi.org/10.1038/s44306-024-00021-8>
- [11] S. D. Ganichev, E. L. Ivchenko, V. V. Bel'kov, S. A. Tarasenko, M. Sollinger, D. Weiss, W. Wegscheider, W. Prettl, Spin-galvanic effect, *Nature* 417 (6885) (2002) 153–156. doi:10.1038/417153a. URL <https://doi.org/10.1038/417153a>
- [12] H. Watanabe, K. Shinohara, T. Nomoto, A. Togo, R. Arita, Symmetry analysis with spin crystallographic groups: Disentangling effects free of spin-orbit coupling in emergent electromagnetism, *Phys. Rev. B* 109 (2024) 094438. doi:10.1103/PhysRevB.109.094438. URL <https://link.aps.org/doi/10.1103/PhysRevB.109.094438>
- [13] P. Wadley, B. Howells, J. Železný, C. Andrews, V. Hills, R. P. Campion, V. Novák, K. Olejník, F. Maccherozzi, S. Dhesi, et al., Electrical switching of an antiferromagnet, *Science* 351 (6273) (2016) 587–590. doi:10.1126/science.aab1031. URL <https://doi.org/10.1126/science.aab1031>
- [14] S. Y. Bodnar, L. Šmejkal, I. Turek, T. Jungwirth, O. Gomonay, J. Sinova, A. A. Sapozhnik, H.-J. Elmers, M. Kläui, M. Jourdan, Writing and reading antiferromagnetic Mn₂Au by Néel spin-orbit torques and large anisotropic magnetoresistance, *Nat. Commun.* 9 (1) (2018) 348. doi:10.1038/s41467-017-02780-x. URL <https://doi.org/10.1038/s41467-017-02780-x>
- [15] A. M. Poletaeva, A. I. Nikitchenko, N. A. Pertsev, Néel Vector Auto-Oscillations and Reorientations Induced by Spin-Polarized Electric Currents in Antiferromagnetic Mn₂Au Nanolayer, *SPIN* 14 (4) (2024) 2450017. doi:10.1142/S2010324724500176. URL <https://doi.org/10.1142/S2010324724500176>
- [16] Z. Kašpar, M. Surýnek, J. Zubáč, F. Krizek, V. Novák, R. P. Campion, M. S. Wörnle, P. Gambardella, X. Marti, P. Němec, K. W. Edmonds, S. Reimers, O. J. Amin, F. Maccherozzi, S. S. Dhesi, P. Wadley, J. Wunderlich, K. Olejník, T. Jungwirth, Quenching of an antiferromagnet into high resistivity states using electrical or ultrashort optical pulses, *Nat. Electron.* 4 (1) (2021) 30–37. doi:10.1038/s41928-020-00506-4. URL <https://doi.org/10.1038/s41928-020-00506-4>
- [17] K. Olejník, Z. Kašpar, J. Zubáč, S. Telkamp, A. Farkaš, D. Krieger, K. Vybourný, J. Železný, Z. Šobán, P. Zeng, et al., Quench switching of Mn₂As, arXiv preprint arXiv:2411.01930 (2024). doi:10.48550/arXiv.2411.01930. URL <https://doi.org/10.48550/arXiv.2411.01930>
- [18] J. Heitz, L. Nádvořník, V. Balos, Y. Behovits, A. Chekhov, T. Seifert, K. Olejník, Z. Kašpar, K. Geishendorf, V. Novák, R. Campion, M. Wolf, T. Jungwirth, T. Kampfrath, Optically Gated Terahertz-Field-Driven Switching of Antiferromagnetic CuMnAs, *Phys. Rev. Appl.* 16 (2021) 064047. doi:10.1103/PhysRevApplied.16.064047. URL <https://link.aps.org/doi/10.1103/PhysRevApplied.16.064047>
- [19] Y. Behovits, A. L. Chekhov, S. Y. Bodnar, O. Gueckstock, S. Reimers, Y. Lytvynenko, Y. Skourski, M. Wolf, T. S. Seifert, O. Gomonay, M. Kläui, M. Jourdan, T. Kampfrath, Terahertz Néel spin-orbit torques drive nonlinear magnon dynamics in antiferromagnetic Mn₂Au, *Nat. Commun.* 14 (1) (2023) 6038. doi:10.1038/s41467-023-41569-z. URL <https://doi.org/10.1038/s41467-023-41569-z>
- [20] P. Wadley, V. Novák, R. Campion, C. Rinaldi, X. Martí, H. Reichlová, J. Železný, J. Gazquez, M. Roldan, M. Varela, D. Khalyavin, S. Langridge, D. Krieger, F. Mäca, J. Mašek, R. Bertacco, V. Holý, A. Rushforth, K. Edmonds, B. Gallagher, C. Foxon, J. Wunderlich, T. Jungwirth, Tetragonal phase of epitaxial room-temperature antiferromagnet CuMnAs, *Nat. Commun.* 4 (1) (2013) 2322. doi:10.1038/ncomms3322. URL <https://doi.org/10.1038/ncomms3322>
- [21] V. M. T. S. Barthem, C. V. Colin, H. Mayaffre, M.-H. Julien, D. Givord, Revealing the properties of Mn₂Au for antiferromagnetic spintronics, *Nat. Commun.* 4 (1) (2013) 2892. doi:10.1038/ncomms3892. URL <https://doi.org/10.1038/ncomms3892>
- [22] P. Wadley, V. Hills, M. R. Shahedkhan, K. W. Edmonds, R. P. Campion, V. Novák, B. Ouladdiaf, D. Khalyavin, S. Langridge, V. Saidl, P. Němec, A. W. Rushforth, B. L. Gallagher, S. S. Dhesi, F. Maccherozzi, J. Železný, T. Jungwirth, Antiferromagnetic structure in tetragonal CuMnAs thin films, *Sci. Rep.* 5 (1) (2015) 17079. doi:10.1038/srep17079. URL <https://doi.org/10.1038/srep17079>
- [23] T. B. Massalski, H. Okamoto, The Au-Mn (Gold-Manganese) system, *Bull. Alloy Phase Diagrams* 6 (5) (1985) 454–467. doi:10.1007/bf02869510. URL <http://dx.doi.org/10.1007/BF02869510>
- [24] M. S. Gebre, R. K. Banner, K. Kang, K. Qu, H. Cao, A. Schleife, D. P. Shoemaker, Magnetic anisotropy in single-crystalline antiferromagnetic Mn₂Au, *Phys. Rev. Mater.* 8 (2024) 084413. doi:10.1103/PhysRevMaterials.8.084413. URL <https://link.aps.org/doi/10.1103/PhysRevMaterials.8.084413>
- [25] M. S. Gebre, R. K. Banner, K. Kang, K. Qu, H. Cao, A. Schleife,

- D. P. Shoemaker, Magnetic anisotropy in single-crystalline antiferromagnetic Mn_2Au , *Phys. Rev. Mater.* 8 (2024) 084413. doi:10.1103/PhysRevMaterials.8.084413.
URL <https://link.aps.org/doi/10.1103/PhysRevMaterials.8.084413>
- [26] S. Reimers, O. Gomonay, O. J. Amin, F. Krizek, L. X. Barton, Y. Lytvynenko, S. F. Poole, V. Novák, R. P. Campion, F. Maccherozzi, G. Carbone, A. Björling, Y. Niu, E. Golias, D. Kriegner, J. Sinova, M. Kläui, M. Jourdan, S. S. Dhesi, K. W. Edmonds, P. Wadley, Magnetic domain engineering in antiferromagnetic CuMnAs and Mn_2Au , *Phys. Rev. Appl.* 21 (2024) 064030. doi:10.1103/PhysRevApplied.21.064030.
URL <https://link.aps.org/doi/10.1103/PhysRevApplied.21.064030>
- [27] A. K. Zvezdin, Dynamics of domain walls in weak ferromagnets, *JETP Lett.* 29 (10) (1979) 553–556.
URL http://jetpletters.ru/ps/1456/article_22180.shtml
- [28] A. K. Zvezdin, Dynamics of domain walls in weak ferromagnets, arXiv preprint arXiv:1703.01502 (2017). doi:arXiv:1703.01502v1.
URL <https://doi.org/10.48550/arXiv.1703.01502>
- [29] A. K. Zvezdin, R. M. Dubrovin, A. V. Kimel, Giant Parametric Amplification of the Inverse Cotton–Mouton Effect in Antiferromagnetic Crystals, *JETP Lett.* 119 (5) (2024) 363–371. doi:10.1134/S0021364023604050.
URL <https://doi.org/10.1134/S0021364023604050>
- [30] E. Fradkin, *Field theories of condensed matter physics*, Cambridge University Press, 2013.
- [31] T. W. Metzger, K. A. Grishunin, C. Reinhofer, R. M. Dubrovin, A. Arshad, I. Ilyakov, T. V. de Oliveira, A. Ponomaryov, J.-C. Deinert, S. Kovalev, R. V. Pisarev, M. I. Katsnelson, B. A. Ivanov, P. H. van Loosdrecht, A. V. Kimel, E. A. Mashkovich, Magnon-phonon fermi resonance in antiferromagnetic CoF_2 , *Nat. Commun.* 15 (1) (2024) 5472. doi:10.1038/s41467-024-49716-w.
URL <https://doi.org/10.1038/s41467-024-49716-w>
- [32] T. G. H. Blank, K. A. Grishunin, K. A. Zvezdin, N. T. Hai, J. C. Wu, S.-H. Su, J.-C. A. Huang, A. K. Zvezdin, A. V. Kimel, Two-dimensional terahertz spectroscopy of nonlinear phononics in the topological insulator MnBi_2Te_4 , *Phys. Rev. Lett.* 131 (2023) 026902. doi:10.1103/PhysRevLett.131.026902.
URL <https://link.aps.org/doi/10.1103/PhysRevLett.131.026902>
- [33] E. A. Mashkovich, K. A. Grishunin, R. M. Dubrovin, A. K. Zvezdin, R. V. Pisarev, A. V. Kimel, Terahertz light-driven coupling of antiferromagnetic spins to lattice, *Science* 374 (2021) 1608–1611. doi:10.1126/science.abk1121.
URL <https://doi.org/10.1126/science.abk1121>
- [34] L. Landau, E. Lifshitz, *Electrodynamics of continuous media*, Vol. 8, Pergamon, 1984.
- [35] A. Thoman, A. Kern, H. Helm, M. Walther, Nanostructured gold films as broadband terahertz antireflection coatings, *Phys. Rev. B* 77 (2008) 195405. doi:10.1103/PhysRevB.77.195405.
URL <https://link.aps.org/doi/10.1103/PhysRevB.77.195405>
- [36] M. Wang, C. Andrews, S. Reimers, O. J. Amin, P. Wadley, R. P. Campion, S. F. Poole, J. Felton, K. W. Edmonds, B. L. Gallagher, A. W. Rushforth, O. Makarovskiy, K. Gas, M. Sawicki, D. Kriegner, J. Zubáč, K. Olejník, V. Novák, T. Jungwirth, M. Shahrokhsand, U. Zeitler, S. S. Dhesi, F. Maccherozzi, Spin flop and crystalline anisotropic magnetoresistance in CuMnAs , *Phys. Rev. B* 101 (2020) 094429. doi:10.1103/PhysRevB.101.094429.
URL <https://link.aps.org/doi/10.1103/PhysRevB.101.094429>
- [37] M. Arana, F. Estrada, D. S. Maior, J. B. S. Mendes, L. E. Fernandez-Outon, W. A. A. Macedo, V. M. T. S. Barthem, D. Givord, A. Azevedo, S. M. Rezende, Observation of magnons in Mn_2Au films by inelastic Brillouin and Raman light scattering, *Appl. Phys. Lett.* 111 (19) (2017). doi:10.1063/1.5001705.
URL <https://doi.org/10.1063/1.5001705>
- [38] N. Bhattacharjee, A. A. Sapozhnik, S. Y. Bodnar, V. Y. Grigorev, S. Y. Agustsson, J. Cao, D. Dominko, M. Obergfell, O. Gomonay, J. Sinova, M. Kläui, H.-J. Elmers, M. Jourdan, J. Demsar, Néel Spin-Orbit Torque Driven Antiferromagnetic Resonance in Mn_2Au Probed by Time-Domain THz Spectroscopy, *Phys. Rev. Lett.* 120 (2018) 237201. doi:10.1103/PhysRevLett.120.237201.
URL <https://link.aps.org/doi/10.1103/PhysRevLett.120.237201>
- [39] A. B. Shick, S. Khmelevskiy, O. N. Mryasov, J. Wunderlich, T. Jungwirth, Spin-orbit coupling induced anisotropy effects in bimetallic antiferromagnets: A route towards antiferromagnetic spintronics, *Phys. Rev. B* 81 (2010) 212409. doi:10.1103/PhysRevB.81.212409.
URL <https://link.aps.org/doi/10.1103/PhysRevB.81.212409>
- [40] D. N. Astrov, The magnetoelectric effect in antiferromagnetics, *Sov. Phys. JETP* 11 (3) (1960) 708–709.
URL http://www.jetp.ras.ru/cgi-bin/dn/e_011_03_0708.pdf
- [41] D. N. Astrov, Magnetoelectric effect in chromium oxide, *Sov. Phys. JETP* 13 (4) (1961) 729–733.
URL http://jetp.ras.ru/cgi-bin/dn/e_013_04_0729.pdf
- [42] G. T. Rado, V. J. Folen, Observation of the Magnetically Induced Magnetoelectric Effect and Evidence for Antiferromagnetic Domains, *Phys. Rev. Lett.* 7 (1961) 310–311. doi:10.1103/PhysRevLett.7.310.
URL <https://link.aps.org/doi/10.1103/PhysRevLett.7.310>
- [43] Y. Tokunaga, S. Iguchi, T. Arima, Y. Tokura, Magnetic-Field-Induced Ferroelectric State in DyFeO_3 , *Phys. Rev. Lett.* 101 (2008) 097205. doi:10.1103/PhysRevLett.101.097205.
URL <https://link.aps.org/doi/10.1103/PhysRevLett.101.097205>
- [44] E. Bousquet, A. Cano, Non-collinear magnetism in multiferroic perovskites, *J. Phys. Condens. Matter* 28 (12) (2016) 123001. doi:10.1088/0953-8984/28/12/123001.
URL <https://doi.org/10.1088/0953-8984/28/12/123001>
- [45] J.-P. Rivera, A short review of the magnetoelectric effect and related experimental techniques on single phase (multi-) ferroics, *Eur. Phys. J. B* 71 (2009) 299–313. doi:10.1140/epjb/e2009-00336-7.
URL <https://doi.org/10.1140/epjb/e2009-00336-7>
- [46] A. F. Andreev, V. I. Marchenko, Symmetry and the macroscopic dynamics of magnetic materials, *Sov. Phys. Usp.* 130 (1980) 39. doi:10.1070/PU1980v023n01ABEH004859.
URL <https://doi.org/10.1070/PU1980v023n01ABEH004859>
- [47] A. K. Zvezdin, A. A. Mukhin, New nonlinear dynamics effects in antiferromagnets, *Bull. Lebedev Phys. Inst.* 12 (1981) 10.
- [48] T. Satoh, S.-J. Cho, R. Iida, T. Shimura, K. Kuroda, H. Ueda, Y. Ueda, B. A. Ivanov, F. Nori, M. Fiebig, Spin Oscillations in Antiferromagnetic NiO Triggered by Circularly Polarized Light, *Phys. Rev. Lett.* 105 (2010) 077402. doi:10.1103/PhysRevLett.105.077402.
URL <https://link.aps.org/doi/10.1103/PhysRevLett.105.077402>
- [49] I. E. Dzyaloshinskii, On the magneto-electrical effects in antiferromagnets, *Sov. Phys. JETP* 10 (1960) 628–629. doi:http://jetp.ras.ru/cgi-bin/dn/e_010_03_0628.pdf.
- [50] J. Železný, H. Gao, K. Výborný, J. Zemen, J. Mašek, A. Manchon, J. Wunderlich, J. Sinova, T. Jungwirth, Relativistic Néel-Order Fields Induced by Electrical Current in Antiferromagnets, *Phys. Rev. Lett.* 113 (2014) 157201. doi:10.1103/PhysRevLett.113.157201.
URL <https://link.aps.org/doi/10.1103/PhysRevLett.113.157201>
- [51] F. Y. Gao, X. Peng, X. Cheng, E. Viñas Boström, D. S. Kim, R. K. Jain, D. Vishnu, K. Raju, R. Sankar, S.-F. Lee, M. A. Sentef, T. Kurumaji, X. Li, P. Tang, A. Rubio, E. Baldini, Giant chiral magnetoelectric oscillations in a van der Waals multiferroic, *Nature* 632 (8024) (2024) 273–279. doi:10.1038/s41586-024-07678-5.
URL <https://doi.org/10.1038/s41586-024-07678-5>
- [52] K.-X. Zhang, G. Park, Y. Lee, B. H. Kim, J.-G. Park, Magnetoelectric effect in van der Waals magnets, *npj Quantum Mater.* 10 (1) (2025) 6. doi:10.1038/s41535-025-00725-y.
URL <https://doi.org/10.1038/s41535-025-00725-y>
- [53] L. Šmejkal, Altermagnetic multiferroics and altermagnetoelectric effect, arXiv preprint arXiv:2411.19928 (2024). doi:10.48550/arXiv.2411.19928.
URL <https://doi.org/10.48550/arXiv.2411.19928>